Advances in Difference Equations
a SpringerOpen Journal

RESEARCH Open Access

On some wavelet solutions of singular differential equations arising in the modeling of chemical and biochemical phenomena

Mo Faheem[1], Arshad Khan[1*] and E.R. El-Zahar[2,3]

*Correspondence:
akhan1234in@rediffmail.com
[1]Department of Mathematics, Jamia Millia Islamia, New Delhi, 110025, India
Full list of author information is available at the end of the article

Abstract

This paper is concerned with the Lane–Emden boundary value problems arising in many real-life problems. Here, we discuss two numerical schemes based on Jacobi and Bernoulli wavelets for the solution of the governing equation of electrohydrodynamic flow in a circular cylindrical conduit, nonlinear heat conduction model in the human head, and non-isothermal reaction–diffusion model equations in a spherical catalyst and a spherical biocatalyst. These methods convert each problem into a system of nonlinear algebraic equations, and on solving them by Newton's method, we get the approximate analytical solution. We also provide the error bounds of our schemes. Furthermore, we also compare our results with the results in the literature. Numerical experiments show the accuracy and reliability of the proposed methods.

MSC: 65L05; 65T60

Keywords: Jacobi wavelet; Bernoulli wavelet; Collocation grids

1 Introduction

The solution of Emden–Fowler type equation is vital because of its numerous applications in engineering and technical problems. There are several phenomena like astrophysics, aerodynamics, stellar structure, chemistry, biochemistry, and many others (see [19, 38, 40, 41]) which can be modeled by the Lane–Emden equation of shape operator w given by [18]

$$u''(z) + \frac{\mathrm{w}}{z}u'(z) + f(u,z) = 0, \quad \mathrm{w} > 0. \tag{1.1}$$

A number of research papers are inclined toward the numerical solution of such type of differential equations. The numerical methods for the solution of Lane–Emden equation based on B-spline have been studied in [24, 30–32]. Homotopy analysis methods and iterative schemes for fast convergence and accuracy of solutions of singular and doubly singular BVPs have been developed in [21, 22, 26, 33]. Roul et al. have dealt with the solution of a class of two-point nonlinear singular boundary value problems with Neumann and Robin

boundary conditions by deploying a high order compact finite difference method [25]. A least square recursive approach together with convergence analysis for solving Lane–Emden type initial value problems has been developed in [27], in which they simply reduce the solution of the original initial value problem to the solution of an integral equation. The B-spline method fails to provide a satisfactory approximation in the presence of singularity; on the other hand, the Adomian decomposition methods (ADM) fail to establish a convergent series solution to strongly nonlinear BVPs. To overcome these shortcomings, Roul came up with the combination of ADM and B-spline collocation methods for accurate solution, see [23]. Madduri and Roul developed a fast converging iterative scheme for the solution of a system of Lane–Emden equations converting them into equivalent Fredholm integral equations and treating them with homotopy analysis method [14]. In this paper, we discuss and solve some mathematical models of the chemical and biochemical phenomena using wavelet methods.

1.1 Model of electrohydrodynamic (EHD) flow in a circular cylindrical conduit

The effect of the electric and magnetic field on fluid has been studied by many researchers. Phenomena involving the conversion of electrical and magnetic energy into kinetic energy are known as electrohydrodynamics (EHD) and magnetohydrodynamics (MHD). The effect of the electric field on fluids gives extra means of controlling flow conditions and has various technical applications such as EHD thruster, EHD flow, heat transfer enhancement, EHD drying and evaporation, and functional electrostatic bowler (EHD pump). EHD pump has been designed for semiconductor cooling [5], electrospray mass spectrometry, and electrospray nanotechnology [45]. The MHD flow has a wide range of applications in the fields of chemistry and biology, for instance, the fabrication in cancer tumor therapy resulting hypothermia, decreasing bleeding in the state of acute injuries, magnetic resonance visualizing, and various other diagnostic experiments [3]. Magneto-hybrid nanofluids flow via mixed convection past a radiative circular cylinder was studied in [4]. The EHD flow of a fluid is modeled by a set of partial differential equations, which can be reduced to an ordinary differential equation as in [16], and results in the following Emden–Fowler type of equation:

$$u''(z) + \frac{1}{z}u'(z) + H^2\left(1 - \frac{u}{1-\alpha u}\right) = 0, \tag{1.2}$$

subject to the boundary conditions

$$u'(0) = 0, \qquad u(1) = 0, \tag{1.3}$$

where $u = -\frac{\bar{u}}{KE_0\alpha}$, $\alpha = \frac{K}{j_0}\frac{\partial p}{\partial z} - 1$.

Here, the pressure gradient $\frac{\partial p}{\partial z}$ is a constant that measures the nonlinearity and $H = \sqrt{\frac{j_0 a^2}{\mu K^2 E_0}}$ is the Hartmann number [16]. A schematic diagram of EHD flow is given in Fig. 1.

Equation (1.2) is a strong nonlinear differential equation having a singularity at $z = 0$. Finding the exact solution to this problem is quite complicated, and therefore the development and use of numerical techniques for the solution of this problem play an important role. Only few numerical methods are available for the solution of (1.2). For instance, Mastroberardino developed homotopy analysis method [15], Ghasemi et al. used least square

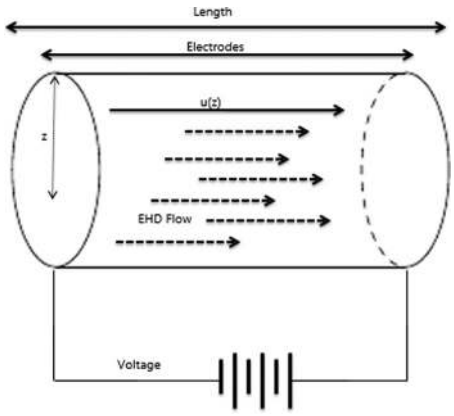

Figure 1 Schematic diagram of EHD flow in a circular cylindrical conduit

method [6], Mosayebidorcheh applied Taylor series [17], and Roul et al. gave a new iterative algorithm [28] for the solution of strongly nonlinear singular boundary value problems.

1.2 Nonlinear heat conduction model in human head

Biomechanics is the area of science in which mechanics laws and formulae are used to study the behavior of the human body. The heat flow in the human body is quivering and vital field that helps to analyze the human heat stress at various temperatures. The human head is the only organ in the human body that controls different parts and functions in the body. The authors in [37] and [13] studied the effect of digital mobile phone emission on the human brain and concluded that the cellular phone waves can cause several brain problems, like exciting the brain cell, weakening the neural behavior, and possible disruption in the functionality of the nervous system. Ketley [11] points out the neuropsychological squeal of digital mobile phone exposure in humans. Similarly, the thermal effect of wave and radiation from digital phones on the human nervous system and brain is studied in [7, 12, 39, 44].

The following Emden-type equation is used to model the distribution of heat source in the human head [2]:

$$u''(z) + \frac{2}{z}u'(z) + \frac{p(u)}{\gamma} = 0, \quad 0 < z < 1, \tag{1.4}$$

subject to the boundary conditions

$$u'(0) = 0, \qquad -\nu u'(1) = \mu(u - u_k), \tag{1.5}$$

where $p(u)$ is the heat production rate per unit volume, u is the absolute temperature, z is the radial distance from the center. Figure 2 shows the schematic diagram of human heat conduction model.

Many researchers have shown their interest in solving this model numerically. For example, Wessapan et al. [43] derived a numerical algorithm of specific absorption rate and heat transfer in the human body to leakage electromagnetic field. Keangin et al. [9] gave an analysis of heat transfer in liver tissue during microwave ablation using single and two double slot antennae. Wessapan and Rattanadecho [42] used a three-dimensional human

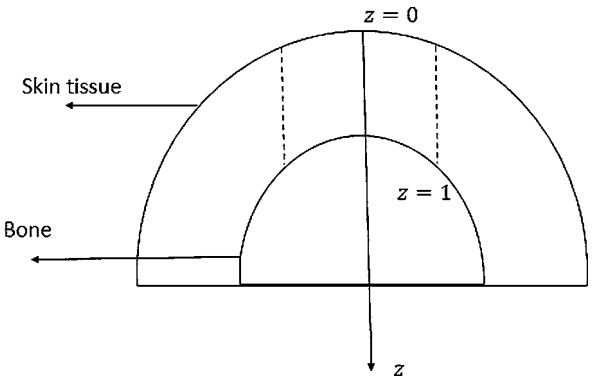

Figure 2 Schematic diagram of human heat conduction model

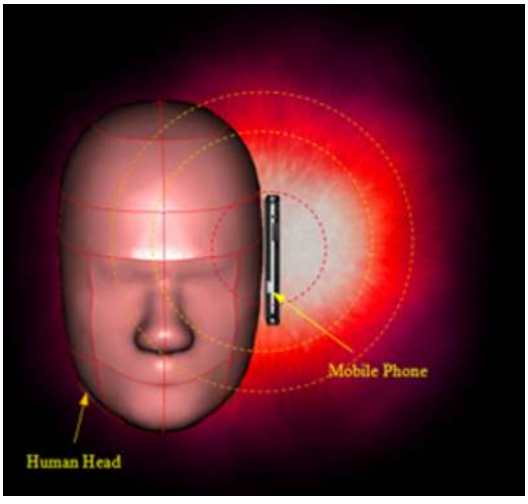

Figure 3 Human head exposed to mobile phone radiation [42]

head model for simulating the heat distribution by applying 3-D finite element mesh (see Fig. 3).

1.3 Mathematical model of spherical catalyst equation

The following Lane–Emden equation is used to model the dimensionless concentration of chemical species which occur in a spherical catalyst [19]:

$$u''(z) + \frac{2}{z}u'(z) - \rho^2 u(z)e^{(\frac{\sigma\beta(1-u(z))}{1+\beta(1-u(z))})} = 0, \tag{1.6}$$

subject to the boundary conditions

$$u'(0) = 0, \quad u(1) = 1, \tag{1.7}$$

where ρ^2, σ, and β denote the Thiele modulus, dimensionless activation energy, and dimensionless heat of reaction, respectively, and are given by

$$\rho^2 = \frac{\kappa_{ref}\mathrm{R}^2}{\mathrm{D}}, \qquad \sigma = \frac{\mathrm{E}}{\mathrm{R_g T_s}}, \qquad \beta = \frac{(-\Delta \mathrm{H})\mathrm{DC_{As}}}{\mathrm{KT_s}}, \qquad z = \frac{\mathrm{R}}{\mathrm{r}}, \quad \text{and} \quad u = \frac{\mathrm{C_A}}{\mathrm{C_{As}}} \quad [19].$$

The effectiveness factor of spherical pellet is defined as [34]

$$\eta = \frac{3}{\rho^2}u'(z) \quad \text{at } z = 1.$$

1.4 Mathematical model of spherical biocatalyst equation

The following Lane–Emden equation is used for modeling the spherical biocatalyst equation [34]:

$$u''(z) + \frac{2}{z}u'(z) - \rho^2\frac{(1+\beta)u(z)}{1+\beta u(z)} = 0, \tag{1.8}$$

subject to the boundary conditions

$$u'(0) = 0, \qquad u(1) = 1, \tag{1.9}$$

where ρ^2, σ, and β denote the Thiele modulus, dimensionless activation energy, and dimensionless heat of reaction, respectively, and are given by

$$\rho^2 = \frac{-\mathrm{r_{As}R}^2}{\mathrm{DD_{As}}}, \qquad \beta = \frac{\mathrm{C_{As}}}{\mathrm{K_m}}, \qquad z = \frac{\mathrm{R}}{\mathrm{r}}, \quad \text{and} \quad u = \frac{\mathrm{C_A}}{\mathrm{C_{As}}} \quad [34].$$

The effectiveness factor of spherical pellet is defined as [34]

$$\eta = \frac{3}{\rho^2}u'(z) \quad \text{at } z = 1.$$

The schematic diagram of spherical biocatalyst is shown in Fig. 4.

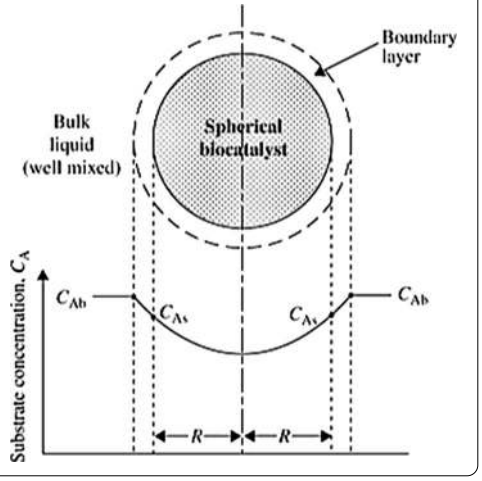

Figure 4 Schematic diagram of spherical biocatalyst

Several numerical techniques have been adopted for solving non-isothermal reaction–diffusion model equations. For instance, Singh [34] applied optimal homotopy analysis method, and Jamal and Khuri [8] used Green's function and fixed point iteration approach for solving such type of equations. Rach et al. [19] reduced this model equation into an equivalent Volterra integral equation and then solved it by coupling the modified Adomian decomposition method and the Volterra integral technique.

Jacobi wavelet is the family of wavelets reduced into Legendre wavelet, Chebyshev wavelet, and Gegenbauer wavelet for the specific value of κ and ω. There are a lot of research papers available for the solution of ordinary and partial differential equations using Jacobi and Bernoulli wavelets, for instance, see [1, 10, 20, 46]. In this study, we introduce two methods based on Jacobi and Bernoulli wavelets for solving models of electrohydrodynamic flow in a circular cylindrical conduit, nonlinear heat conduction model in the human head, spherical catalyst equation, and spherical biocatalyst equation. These wavelets transform these model equations into a system of nonlinear algebraic equations, and on solving them, we get the unknown wavelet coefficients. With the help of these coefficients, we get the approximate analytical solution that is valid over all the problem domain, not only at grid points. The outline of this paper is as follows: The second section describes the Jacobi wavelet, function approximation by Jacobi wavelet, and integration of Jacobi wavelet. Similarly, the third section describes the Bernoulli wavelet, function approximation by Bernoulli wavelet, and integration of Bernoulli wavelet. In the fourth section, the wavelet approximation method for all the above models is given. In the fifth section, we state some theoretical proof for error bounds of our methods. In the sixth section, the numerical experiments confirm that our methods converge fast.

2 Jacobi wavelet

2.1 Jacobi polynomials

Jacobi polynomials, which are often called hypergeometric polynomials, are denoted by $\jmath_m^{\kappa,\omega}(z)$ and can be defined by the following explicit formula:

$$\jmath_m^{\kappa,\omega}(z) = \frac{\Gamma(\kappa+m+1)}{m!\Gamma(\kappa+\omega+m+1)} \sum_{i=0}^{m} \binom{m}{i} \frac{\Gamma(\kappa+\omega+i+m+1)}{\Gamma(\kappa+i+1)} \left(\frac{z-1}{2}\right)^i.$$

Some first few Jacobi polynomials are given by

$$\begin{aligned}
&\jmath_0^{\kappa,\omega}(z) = 1,\\
&\jmath_1^{\kappa,\omega}(z) = \kappa+1+(\kappa+\omega+2)\frac{z-1}{2},\\
&\jmath_2^{\kappa,\omega}(z) = \frac{(\kappa+1)(\kappa+2)}{2} + (\kappa+2)(\kappa+\omega+3)\frac{z-1}{2}\\
&\qquad + \frac{(\kappa+\omega+3)(\kappa+\omega+4)}{2}\left(\frac{z-1}{2}\right)^2, \qquad \ldots.
\end{aligned}$$

These polynomials are orthogonal on $[-1, 1]$ with respect to the weight $(1-z)^\kappa(1-z)^\omega$ and satisfy the following properties:

$$\jmath_m^{\kappa,\omega}(-1) = (-1)^m \binom{m+\omega}{m},$$

$$\mathfrak{J}_m^{\kappa,\omega}(-z) = (-1)^m \mathfrak{J}_m^{\omega,\kappa}(z),$$

$$\mathfrak{J}_m^{\kappa,\kappa}(z) = \begin{cases} \frac{\Gamma(m+\kappa+1)\Gamma(\frac{m}{2}+1)}{\Gamma(\frac{m}{2}+\kappa+1)\Gamma(m+1)} \mathfrak{J}_{\frac{m}{2}}^{\kappa,\frac{-1}{2}}(2z^2-1), & \text{if } m \text{ is even,} \\ \frac{\Gamma(m+\kappa+2)\Gamma(\frac{m}{2}+1)}{\Gamma(\frac{m}{2}+\kappa+1)\Gamma(m+2)} z\mathfrak{J}_{\frac{m}{2}}^{\kappa,\frac{1}{2}}(2z^2-1), & \text{if } m \text{ is odd.} \end{cases}$$

$$\int_{-1}^{1} (1-z)^{\kappa}(1+z)^{\omega} \mathfrak{J}_m^{\kappa,\omega}(z)\mathfrak{J}_n^{\kappa,\omega}(z)\,dz = \frac{2^{\kappa+\omega+1}}{2m+\kappa+\omega+1} \frac{\Gamma(m+\kappa+1)\Gamma(m+\omega+1)}{\Gamma(m+\kappa+\omega+1)m!}\delta_{nm},$$

where δ_{nm} is Kronecker delta.

$$\begin{aligned} &2m(m+\kappa+\omega)(2m+\kappa+\omega-2)J_m^{\kappa,\omega}(z) \\ &\quad = (2m+\kappa+\omega-1)\big((2m+\kappa+\omega)(2m+\kappa+\omega-2)z \\ &\qquad + \kappa^2-\omega^2\big)\mathfrak{J}_{m-1}^{\kappa,\omega}(z) - 2(m+\alpha-1)(m+\omega-1)(2m+\kappa+\omega)\mathfrak{J}_{m-2}^{\kappa,\omega}(z). \end{aligned}$$

2.2 Jacobi wavelet of shifted Jacobi polynomial

Jacobi wavelet of the shifted Jacobi polynomial defined on six arguments $k, n, \kappa, \omega, m, z$ is denoted by $\mathcal{J}(k,n,\kappa,\omega,m,z) = \mathcal{J}_{n,m}^{\kappa,\omega}(z)$, and can be defined on $[0, 1)$ as follows [1]:

$$\mathcal{J}_{n,m}^{\kappa,\omega}(z) = \begin{cases} 2^{\frac{k}{2}}\mu_m^{\kappa,\omega}\mathfrak{J}_m^{\kappa,\omega}(2^k z-2n+1), & \text{if } z \in [\xi_1,\xi_2), \\ 0, & \text{otherwise,} \end{cases} \tag{2.1}$$

where $\xi_1 = \frac{n-1}{2^{k-1}}$, $\xi_2 = \frac{n}{2^{k-1}}$, and $\mu_m^{\kappa,\omega} = \sqrt{\frac{(2m+\kappa+\omega+1)\Gamma(2m+\kappa+\omega+1)m!}{2^{\kappa+\omega+1}\Gamma(m+\kappa+1)\Gamma(m+\omega+1)}}$.

Equivalently, for any positive integer k, Jacobi wavelet can also be defined as follows:

$$\mathcal{J}_i^{\kappa,\omega}(z) = \begin{cases} 2^{\frac{k}{2}}\mu_m^{\kappa,\omega}\mathfrak{J}_m^{\kappa,\omega}(2^k z-2n+1), & \text{if } z \in [\xi_1,\xi_2), \\ 0, & \text{otherwise,} \end{cases} \tag{2.2}$$

where i is wavelet number determined by $i = n + 2^{k-1}m$, where $n = 0, 1, 2, \ldots$ and $m = 0, 1, 2, \ldots, M-1$, where m is degree of polynomial. M can be determined by $M = \frac{N}{2^{k-1}}$, where $k = 1, 2, \ldots$.

2.2.1 Function approximation by Jacobi wavelet

Let $\{\mathcal{J}_{1,0}^{\kappa,\omega}, \ldots, \mathcal{J}_{1,M-1}^{\kappa,\omega}, \mathcal{J}_{2,0}^{\kappa,\omega}, \ldots, \mathcal{J}_{2,M-1}^{\kappa,\omega}, \mathcal{J}_{2^{k-1},0}^{\kappa,\omega}, \ldots, \mathcal{J}_{2^{k-1},M-1}^{\kappa,\omega}\}$ be a set of Jacobi wavelets.

Any function $f(z) \in L^2[0,1)$ can be expressed in terms of Jacobi wavelet as follows [1]:

$$f(z) = \sum_{n=1}^{\infty}\sum_{m=0}^{\infty} a_{n,m}\mathcal{J}_{n,m}^{\kappa,\omega}(z) = \sum_{i=1}^{\infty} a_i \mathcal{J}_i^{\kappa,\omega}(z).$$

For approximation, we truncate this series for a natural number N, and we get

$$f(z) \approx \sum_{n=1}^{2^{k-1}}\sum_{m=0}^{M-1} a_{n,m}\mathcal{J}_{n,m}^{\kappa,\omega}(z) = \sum_{i=1}^{N} a_i \mathcal{J}_i^{\kappa,\omega}(z) \tag{2.3}$$

$$= a^T \mathcal{J}(z), \tag{2.4}$$

where a and $\mathcal{J}(z)$ are matrices of order $N \times 1$ given by

$$\begin{aligned} a &= [a_{1,0}, a_{1,1}, \ldots, a_{1,M-1}, a_{2,0}, a_{2,1}, \ldots, a_{2,M-1}, \ldots, a_{2^{k-1},0}, \ldots, a_{2^{k-1},M-1}]^T \\ &= [a_1, a_2, \ldots, a_N]^T, \end{aligned} \tag{2.5}$$

$$\begin{aligned} \mathcal{J}(z) &= \left[\mathcal{J}_{1,0}^{\kappa,\omega}(z), \ldots, \mathcal{J}_{1,M-1}^{\kappa,\omega}(z), \mathcal{J}_{2,0}^{\kappa,\omega}(z), \ldots, \mathcal{J}_{2,M-1}^{\kappa,\omega}(z), \mathcal{J}_{2^{k-1},0}^{\kappa,\omega}(z), \ldots, \mathcal{J}_{2^{k-1},M-1}^{\kappa,\omega}(z)\right] \\ &= \left[\mathcal{J}_1^{\kappa,\omega}(z), \ldots, \mathcal{J}_N^{\kappa,\omega}(z)\right], \end{aligned} \tag{2.6}$$

where the coefficient a_i can be determined by $a_i = \langle f(z), \mathcal{J}_i^{\kappa,\omega}(z)\rangle = \int_0^1 f(z)\overline{\mathcal{J}_i^{\kappa,\omega}(z)}\,dz$.

2.2.2 Integration of Jacobi wavelet

Let $\mathcal{J}_i^1(z)$, $\mathcal{J}_i^2(z)$, and $\mathcal{J}_i^3(z)$ be the first, second, and third integration of Jacobi wavelet from 0 to z respectively. These integrations can be determined as follows:

$$\mathcal{J}_{1,i}^{\kappa,\omega}(z) = \begin{cases} 2^{\frac{-k}{2}}\mu_m^{\kappa,\omega}(\frac{1}{(m+\kappa+\omega)})\{\mathfrak{I}_{m+1}^{\kappa-1,\omega-1}(\hat{z}) - \mathfrak{I}_{m+1}^{\kappa-1,\omega-1}(-1)\}, & \xi_1 \le z < \xi_2, \\ 2^{\frac{-k}{2}}\mu_m^{\kappa,\omega}(\frac{1}{(m+\kappa+\omega)})\{\mathfrak{I}_{m+1}^{\kappa-1,\omega-1}(1) - \mathfrak{I}_{m+1}^{\kappa-1,\omega-1}(-1)\}, & \xi_2 \le z \le 1, \end{cases} \tag{2.7}$$

$$\mathcal{J}_{2,i}^{\kappa,\omega}(z) = \begin{cases} 2^{\frac{-3k}{2}}\mu_m^{\kappa,\omega}(\frac{1}{(m+\kappa+\omega)})\{(\frac{1}{(m-2+\kappa+\omega)})\{\mathfrak{I}_{m+2}^{\kappa-2,\omega-2}(\hat{z}) \\ \quad - \mathfrak{I}_{m+2}^{\kappa-2,\omega-2}(-1)\} - (1+\hat{z})\mathfrak{I}_{m+1}^{\kappa-1,\omega-1}(-1)\}, & \xi_1 \le z < \xi_2, \\ 2^{\frac{-3k}{2}}\mu_m^{\kappa,\omega}(\frac{1}{(m+\kappa+\omega)})\{(\frac{1}{(m-2+\kappa+\omega)})\{\mathfrak{I}_{m+2}^{\kappa-2,\omega-2}(1) \\ \quad - \mathfrak{I}_{m+2}^{\kappa-2,\omega-2}(-1)\} - 2\mathfrak{I}_{m+1}^{\kappa-1,\omega-1}(-1) \\ \quad + (\hat{z}-1)\{\mathfrak{I}_{m+1}^{\kappa-1,\omega-1}(1) - \mathfrak{I}_{m+1}^{\kappa-1,\omega-1}(-1)\}\}, & \xi_2 \le z \le 1, \end{cases} \tag{2.8}$$

where $\hat{z} = 2^k z - 2n + 1$.

3 Bernoulli wavelet

3.1 Bernoulli polynomials

Bernoulli polynomials are denoted by $ß_m(z)$, where m is the degree of polynomials and can be defined by the following explicit formula:

$$ß_m(z) = \sum_{i=0}^{m} \binom{m}{i} ß_{m-i} z^i,$$

where $ß_k, k = 0, 1, 2, \ldots m$, are the Bernoulli numbers. Another explicit formula for these polynomials is given by

$$ß_m(z) = \sum_{i=0}^{m} \frac{1}{i+1} \sum_{j=0}^{i} (-1)^j \binom{i}{j} (z+j)^m.$$

The first few Bernoulli polynomials are given by

$$ß_0(z) = 1, \qquad ß_1(z) = z - \frac{1}{2}, \qquad ß_2(z) = z^2 - z + \frac{1}{6}, \qquad ß_3(z) = z^3 - \frac{3}{2}z^2 + \frac{1}{2}z.$$

Bernoulli polynomial satisfies the following properties:

$$ß_m(1) = (-1)^m ß_m(0),$$

$$ß_{2m+1}(0) = 0, \qquad ß_{2m-1}\left(\frac{1}{2}\right) = 0,$$

$$ß_m(1-z) = (-1)^m ß_m(z),$$

$$ß_m(z+1) - ß_m(z) = mz^{m-1},$$

$$\int_0^1 ß_n(z)ß_m(z)\,dz = (-1)^{n-1}\frac{n!m!}{(m+n)!}ß_{m+n}.$$

Bernoulli polynomials can be calculated by the following recursive formula: $ß'_m(z) = m ß_{m-1}(z)$.

3.2 Bernoulli wavelet

Bernoulli wavelet defined on four arguments k, n, m, z is denoted by $\mathcal{B}(k,n,m,z) = \mathcal{B}_{n,m}(z)$ and can be defined on [0,1) as follows [10]:

$$\mathcal{B}_{n,m}(z) = \begin{cases} 2^{\frac{k-1}{2}}\overline{ß}_m(2^{k-1}z - n + 1), & \xi_1 \le z \le \xi_2, \\ 0, & \text{elsewhere,} \end{cases} \tag{3.1}$$

where $\xi_1 = \frac{n-1}{2^{k-1}}$ and $\xi_2 = \frac{n}{2^{k-1}}$ and

$$\overline{ß_m}(z) = \begin{cases} 1, & m = 0, \\ \frac{1}{\sqrt{\frac{(-1)^{m-1}(m!)^2}{(2m)!}ß_{2m}}}ß_m(z), & m > 0, \end{cases} \tag{3.2}$$

where $ß_{2m}$ is the Bernoulli number.

On the interval $[0,1)$, for any positive integer k, Bernoulli wavelet can also be defined as follows:

$$\mathcal{B}_i(z) = \begin{cases} 2^{\frac{k-1}{2}}\overline{ß}_m(2^{k-1}z - n + 1), & \xi_1 \le z \le \xi_2, \\ 0, & \text{elsewhere.} \end{cases} \tag{3.3}$$

Here, i is wavelet number and can calculated by the relation $i = n + 2^{k-1}m$, where $n = 0,1,2,\ldots$ and $m = 0,1,2,\ldots,M-1$, m is degree of polynomials. For $k = 1,2,\ldots,M$ can be found by $N = 2^{k-1}M$.

3.2.1 Function approximation by Bernoulli wavelet

Let $\{\mathcal{B}_{1,0},\ldots,\mathcal{B}_{1,M-1},\mathcal{B}_{2,0},\ldots,\mathcal{B}_{2,M-1},\mathcal{B}_{2^{k-1},0},\ldots,\mathcal{B}_{2^{k-1},M-1}\}$ be a set of Bernoulli wavelets.

Any function $f(z) \in L^2[0,1)$ can be expressed in terms of Bernoulli wavelet as follows [46]:

$$f(z) = \sum_{n=1}^{\infty}\sum_{m=0}^{\infty} b_{n,m}\mathcal{B}_{n,m}(z) = \sum_{i=1}^{\infty} b_i\mathcal{B}_i(z).$$

For approximation, we truncate this series for a natural number N, and we get

$$f(z) \approx \sum_{n=1}^{2^{k-1}}\sum_{m=0}^{M-1} b_{n,m}\mathcal{B}_{n,m}(z) = \sum_{i=1}^{N} b_i\mathcal{B}_i(z) \tag{3.4}$$

$$= b^T \mathcal{B}(z), \tag{3.5}$$

where b and $\mathcal{B}(z)$ are matrices of order $N \times 1$ given by

$$\begin{aligned} b &= [b_{1,0}, b_{1,1}, \ldots, b_{1,M-1}, b_{2,0}, b_{2,1}, \ldots, b_{2,M-1}, \ldots, b_{2^{k-1},0}, \ldots, b_{2^{k-1},M-1}]^T \\ &= [b_1, b_2, \ldots, b_N]^T, \end{aligned} \tag{3.6}$$

$$\begin{aligned} \mathcal{B}(z) &= \left[\mathcal{B}_{1,0}(z), \ldots, \mathcal{B}_{1,M-1}(z), \mathcal{B}_{2,0}(z), \ldots, \mathcal{B}_{2,M-1}(z), \mathcal{B}_{2^{k-1},0}(z), \ldots, \mathcal{B}_{2^{k-1},M-1}(z)\right] \\ &= \left[\mathcal{B}_1(z), \ldots, \mathcal{B}_N(z)\right]. \end{aligned} \tag{3.7}$$

The coefficient b_i is calculated by $b_i = \langle f(z), \mathcal{B}_i(z)\rangle = \int_0^1 f(z)\overline{\mathcal{B}_i(z)}\,dz$.

3.2.2 Integration of Bernoulli wavelet

Let $\mathcal{B}_{1,i}(z)$ and $\mathcal{B}_{2,i}(z)$ be the first and second integration of Bernoulli wavelet from 0 to z, respectively. These integration can be determined as follows:

$$\mathcal{B}_{1,i}(z) = \begin{cases} 2^{\frac{-k+1}{2}}\zeta\left(\frac{1}{m+1}\right)\{ß_{m+1}(\hat{z}) - ß_{m+1}(0)\}, & \xi_1 \le z < \xi_2, \\ 2^{\frac{-k+1}{2}}\zeta\left(\frac{1}{m+1}\right)\{ß_{m+1}(1) - ß_{m+1}(0)\}, & \xi_2 \le z \le 1, \end{cases} \tag{3.8}$$

$$\mathcal{B}_{2,i}(z) = \begin{cases} 2^{\frac{-3k+3}{2}}\zeta\left(\frac{1}{m+1}\right)\left\{\left(\frac{1}{m+2}\right)\{ß_{m+2}(\hat{z}) - ß_{m+2}(0)\} - (\hat{z})ß_{m+1}(0)\right\}, & \xi_1 \le z < \xi_2, \\ 2^{\frac{-3k+3}{2}}\zeta\left(\frac{1}{m+1}\right)\left\{\left(\frac{1}{m+2}\right)\{ß_{m+2}(1) - ß_{m+2}(0)\} - 2ß_{m+1}(0)\right. \\ \quad \left. + (\hat{z}-1)\{ß_{m+1}(1) - ß_{m+1}(0)\}\right\}, & \xi_2 \le z \le 1, \end{cases} \tag{3.9}$$

where $\hat{z} = 2^{k-1}z - n + 1$ and $\zeta = \frac{1}{\sqrt{\frac{(-1)^{m-1}(m!)^2}{(2m)!}ß_{2m}}}$.

4 Methods for solution

In this section, we discuss the methods for the solution of the models described above. The following notations have been introduced:

$$\phi_{1,i}(z) = \int_0^z \phi_i(z)\,dz, \tag{4.1}$$

$$\phi_{2,i}(z) = \int_0^z \phi_{1,i}(z)\,dz, \tag{4.2}$$

$$\Phi_{1,i} = \int_0^1 \phi_{1,i}(z)\,dz, \tag{4.3}$$

$$\Phi_{2,i} = \int_0^1 \phi_{2,i}(z)\,dz. \tag{4.4}$$

4.1 Method for solution of model of electrohydrodynamic flow in a circular cylindrical conduit

We can express the second derivative of (1.2) in terms of wavelet series as follows:

$$u''(z) = \sum_{i=1}^{N} c_i\phi_i(z). \tag{4.5}$$

Integrating (4.5) twice from 0 to z, we get

$$u'(z) = \sum_{i=1}^{N} c_i \phi_{1,i}(z) + u'(0), \tag{4.6}$$

$$u(z) = \sum_{i=1}^{N} c_i \phi_{2,i}(z) + z u'(0) + u(0). \tag{4.7}$$

Using boundary conditions (1.3) in (4.6)–(4.7), we get

$$u'(z) = \sum_{i=1}^{N} c_i \phi_{1,i}(z), \tag{4.8}$$

$$u(z) = \sum_{i=1}^{N} c_i \phi_{2,i}(z) + u(0). \tag{4.9}$$

Putting $z = 1$ in (4.9) and after simplifying, we get

$$u(0) = -\sum_{i=1}^{N} c_i \Phi_{2,i}. \tag{4.10}$$

Therefore equation (4.9) becomes

$$u(z) = \sum_{i=1}^{N} c_i \big(\phi_{2,i}(z) - \Phi_{2,i}\big). \tag{4.11}$$

Putting the values of $u(z)$, $u'(z)$, and $u''(z)$ from equations (4.5), (4.8), (4.11) in equation (1.2) and collocating at $z = z_l = \frac{l-0.5}{N}$, where $l = 1, 2, \ldots, N$, yields the following system of nonlinear equations:

$$\sum_{i=1}^{N} c_i \phi_i(z_l) + \frac{1}{z_l} \sum_{i=1}^{N} c_i \phi_{1,i}(z_l) + \mathrm{H}^2 \left(1 - \frac{\sum_{i=1}^{N} c_i (\phi_{2,i}(z_l) - \Phi_{2,i})}{1 - \alpha \sum_{i=1}^{N} c_i (\phi_{2,i}(z_l) - \Phi_{2,i})}\right) = 0. \tag{4.12}$$

On solving this system of nonlinear equations by Newton's method, we get the unknown wavelet coefficients c_i's. After putting these c_i's in equation (4.11), we get the approximate solution.

4.2 Method for solution of nonlinear heat conduction model in the human head

We can approximate the second derivative of equation (1.4) in terms of wavelet series as follows:

$$u''(z) = \sum_{i=1}^{N} c_i \phi_i(z). \tag{4.13}$$

Integrating (4.13) twice from 0 to z, we get

$$u'(z) = \sum_{i=1}^{N} c_i \phi_{1,i}(z) + u'(0), \tag{4.14}$$

$$u(z) = \sum_{i=1}^{N} c_i \phi_{2,i}(z) + z u'(0) + u(0). \tag{4.15}$$

Using boundary conditions (1.5) in (4.14)–(4.15), we get

$$u'(z) = \sum_{i=1}^{N} c_i \phi_{1,i}(z), \tag{4.16}$$

$$u(z) = \sum_{i=1}^{N} c_i \phi_{2,i}(z) + u(0). \tag{4.17}$$

Putting $z = 1$ in (4.16)–(4.17) and multiplying (4.16) by ν and (4.17) by μ and after solving these equations for $u(0)$, we get

$$u(0) = u_\kappa - \frac{1}{\mu} \sum_{i=1}^{N} c_i (\nu \Phi_{1,i} + \mu \Phi_{2,i}). \tag{4.18}$$

Therefore equation (4.17) becomes

$$u(z) = \sum_{i=1}^{N} c_i \left(\phi_{2,i}(z) - \frac{1}{\mu} (\nu \Phi_{1,i} + \mu \Phi_{2,i}) \right) + u_\kappa. \tag{4.19}$$

Putting the values of $u''(z)$, $u'(z)$, and $u(z)$ from equations (4.13), (4.16), (4.19) in equation (1.4) and collocating at $z = z_l = \frac{l-0.5}{N}$, where $l = 1, 2, \ldots, N$, yields the following system of nonlinear equations:

$$\sum_{i=1}^{N} c_i \phi_i(z_l) + \frac{2}{z_l} \sum_{i=1}^{N} c_i \phi_{1,i}(z_l) + \frac{p(\sum_{i=1}^{N} c_i (\phi_{2,i}(z_l) - \frac{1}{\mu}(\nu \Phi_{1,i} + \mu \Phi_{2,i})) + u_\kappa)}{\gamma} = 0. \tag{4.20}$$

After solving this system of nonlinear equations by Newton's method, we get the unknown wavelet coefficients. On putting these coefficients in equation (4.19), we get the approximate wavelet solutions of nonlinear heat conduction model in the human head.

4.3 Method for solution of spherical catalyst equation

We can approximate the second derivative of equation (1.6) in terms of wavelet series as follows:

$$u''(z) = \sum_{i=1}^{N} c_i \phi_i(z). \tag{4.21}$$

Integrating (4.21) twice from 0 to z, we get

$$u'(z) = \sum_{i=1}^{N} c_i \phi_{1,i}(z) + u'(0), \tag{4.22}$$

$$u(z) = \sum_{i=1}^{N} c_i \phi_{2,i}(z) + z u'(0) + u(0). \tag{4.23}$$

Using boundary conditions (1.7) in (4.22)–(4.23), we get

$$u'(z) = \sum_{i=1}^{N} c_i \phi_{1,i}(z), \tag{4.24}$$

$$u(z) = \sum_{i=1}^{N} c_i \phi_{2,i}(z) + u(0). \tag{4.25}$$

Putting $z = 1$ in (4.25) and after simplification, we get

$$u(0) = 1 - \sum_{i=1}^{N} c_i \Phi_{2,i}. \tag{4.26}$$

Therefore equation (4.25) becomes

$$u(z) = \sum_{i=1}^{N} c_i \big(\phi_{2,i}(z) - \Phi_{2,i}\big) + 1. \tag{4.27}$$

Putting the values of $u''(z)$, $u'(z)$, and $u(z)$ from equations (4.21,4.24,4.27) in equation (1.6) and collocating at $z = z_l = \frac{l-0.5}{N}$, where $l = 1, 2, \ldots, N$, yields the following system of nonlinear equations:

$$\begin{aligned} &\sum_{i=1}^{N} c_i \phi_i(z_l) + \frac{2}{z_l} \sum_{i=1}^{N} c_i \phi_{1,i}(z_l) \\ &\quad - \rho^2 \left(\sum_{i=1}^{N} c_i \big(\phi_{2,i}(z_l) - \Phi_{2,i}\big) + 1 \right) e^{\left\{ \frac{\gamma\beta(1-(\sum_{i=1}^{N} c_i(\phi_{2,i}(z_l)-\Phi_{2,i})+1))}{1+\beta(1-(\sum_{i=1}^{N} c_i(\phi_{2,i}(z_l)-\Phi_{2,i})+1))} \right\}} = 0. \end{aligned} \tag{4.28}$$

After solving this system of nonlinear equations by Newton's method, we get the unknown wavelet coefficients c_i's. On putting these c_i's in equation (4.27), we get the approximate wavelet solutions of spherical catalyst equation.

4.4 Method for solution of spherical biocatalyst equation

The same procedure has been implemented as in case of spherical catalyst equation. Substituting the values of $u''(z)$, $u'(z)$, and $u(z)$ from equations (4.21), (4.24), (4.27) in equation (1.8) and collocating at $z = z_l = \frac{l-0.5}{N}$, where $l = 1, 2, \ldots, N$, yields the following system of nonlinear equations:

$$\sum_{i=1}^{N} c_i \phi_i(z_l) + \frac{2}{z_l} \sum_{i=1}^{N} c_i \phi_{1,i}(z_l) - \rho^2 \frac{(1+\beta)(\sum_{i=1}^{N} c_i(\phi_{2,i}(z_l) - \Phi_{2,i}) + 1)}{1 + \beta(\sum_{i=1}^{N} c_i(\phi_{2,i}(z_l) - \Phi_{2,i}) + 1)} = 0. \tag{4.29}$$

Solving this system of nonlinear equations, we get the unknown wavelet coefficients c_i's. After putting the values of c_i's in equation (4.27), we get the approximate wavelet solutions of spherical biocatalyst equation.

5 Error bounds

Lemma 5.1 *Let* $u(z) \in C^M[0,1]$ *with* $|u^M(z)| \leq \lambda$, $\forall z \in (0,1); \alpha > 0$ *and* $u(z) \simeq \sum_{n=1}^{2^{k-1}} \sum_{m=0}^{M-1} a_{n,m}\phi_{n,m}(z) = \sum_{i=0}^{N} a_i\phi_i(z)$, *where* $\phi_{n,m}(z)$ *is Jacobi or Bernoulli wavelet. Then* $|a_i| \leq \alpha_M 2^{-m(M+\frac{1}{2})}\lambda$.

Lemma 5.2 *Let* $u(z) \in C^M[0,1]$ *and* $u(z) \simeq \sum_{n=1}^{2^{k-1}} \sum_{m=0}^{M-1} a_{n,m}\phi_{n,m}(z) = \sum_{i=0}^{N} a_i\phi_i(z)$. *Let* $\varepsilon_m(z)$ *be the error of approximation. Then* $|\varepsilon_m(z)| \leq \alpha_M \frac{2^{-mM}}{1-2^{-m}}(\frac{M}{2} - 1)\lambda\alpha_\Phi$.

Proof $\varepsilon_m(z) = u(z) - P_{V_m}u(z) = \sum_{m=M}^{\infty} \sum_{n=2^{k-1}+1}^{\infty} a_{n,m}\phi_{n,m}(z)$, $z \in R$ and $|\varepsilon_m(z)| \leq \sum_{m=M}^{\infty} \sum_{n=2^{k-1}+1}^{\infty} |a_{n,m}\phi_{n,m}(z)|$, $z \in R$.

Using Lemma 5.1, we get

$$\left|\varepsilon_m(z)\right| \leq \sum_{m=M}^{\infty} \sum_{n=2^{k-1}+1}^{\infty} \alpha_M 2^{-m(M+\frac{1}{2})} \max_{z\in I_n^m} \left|u^M(z)\right| 2^{\frac{m}{2}} \alpha_\phi,$$

where $\alpha_\phi = \max_{z\in I_n^m} |\phi(2^m z - n)|$.

$$\left|\varepsilon_m(z)\right| \leq \sum_{m=M}^{\infty} \alpha_M 2^{-mM}(2M-1) \max_{z\in I_n^m} \left|g^M(z)\right| \alpha_{\phi G}.$$

For very large m, $|\varepsilon_m(z)| \leq \alpha_M \frac{2^{-mM}}{1-2^{-m}}(2M-1)\lambda\alpha_\phi$, where $\lambda = \max_{z\in I_n^m} |g^M(z)|$. □

Theorem 5.3 *Let* $u(z)$ *be the exact solution of* (1.2), (1.4), (1.6), *and* (1.8) *and* $u_N(z)$ *be the approximate solution, and let* $\varepsilon_m(z)$ *be the error of approximation. Then* $|\varepsilon_m(z)| = O(2^{-mM})$.

Proof Here, we calculate the error bounds for solution of (1.2). The same procedure can be applied for equations (1.4), (1.6), and (1.8).

The error is given by

$$\left|\varepsilon_m(z)\right| = \left|u(z) - u_N(z)\right| = \left|\sum_{m=M}^{\infty} \sum_{n=2^{k-1}+1}^{\infty} a_{n,m}\left(\phi_{n,m}^2(z) - \Phi_{n,m}^1\right)\right|, \tag{5.1}$$

where $\phi_{n,m}^2(z)$ is the second integration of $\phi_{n,m}(z)$ from 0 to z and $\Phi_{n,m}^1$ denotes the second integration of $\phi_{n,m}(z)$ from 0 to 1. Therefore,

$$\left|\varepsilon_m(z)\right| \leq \sum_{m=M}^{\infty} \sum_{n=2^{k-1}+1}^{\infty} \left|a_{n,m}\left(\phi_{n,m}^2(z) - \Phi_{n,m}^1\right)\right|. \tag{5.2}$$

Using Lemma 5.1, we get

$$\left|\varepsilon_m(z)\right| \leq \sum_{m=M}^{\infty} \sum_{n=2^{k-1}+1}^{\infty} \alpha_M 2^{-m(M+\frac{1}{2})} \left|\left(\phi_{n,m}^2(z) - \Phi_{n,m}^1\right)\right| \tag{5.3}$$

$$= \sum_{m=M}^{\infty} \sum_{n=2^{k-1}+1}^{\infty} \alpha_M 2^{-m(M+\frac{1}{2})} 2^{\frac{m}{2}} \left|\left(\phi^2\left(2^m z - n\right) - \Phi_{n,m}^1\right)\right| \tag{5.4}$$

$$\leq \sum_{m=M}^{\infty} \alpha_M 2^{-mM}(2M-1)\lambda\gamma_\phi, \tag{5.5}$$

where $\gamma_\phi = \max_{z\in I_n^m} |(\phi^2(2^m z - n) - \Phi_{n,m}^1)|$. Hence $|\varepsilon_m(z)| = O(2^{-mM})$. □

It is clear that each of the Jacobi and Bernoulli wavelet methods has an exponential rate of convergence/spectral accuracy.

6 Numerical simulation

In this section, we solve the examples of electrohydrodynamic model flow in a circular cylindrical conduit, nonlinear heat conduction model in the human head, spherical catalyst equation, and spherical biocatalyst equation. For the sake of comparison, the resultant approximate analytical solution has been used to find the solution at any point in the interval $[0, 1]$. We have chosen the initial guess as a zero vector of length N. We have used optimality tolerance = 10^{-06} and function tolerance = 10^{-03} in stopping criteria for Newton's method.

6.1 Numerical treatment of EHM equation

We applied Bernoulli wavelet series method (BWSM) and Jacobi wavelet series method (JWSM) ($\kappa = -\frac{3}{7}, \omega = -\frac{1}{8}$) for the solution of (1.2). First we study the effect of nonlinearity (α) on the velocity profile at small value of the Hartmann number (H) and observe that as we increase H, the velocity profile becomes flatter near to the center, see Fig. 5. For small value of H, the velocity profile almost remains parabolic with change in α, see Fig. 6. We also study the influence of different H with fixed α and see that a strong boundary layer is build up in velocity for a large value of H, see Figs. 7 and 8. We see that BWSM result for fixed values $H^2 = 2, 100$ with different value of $\alpha = 0.1, 0.5, 1$ and for fixed values of $\alpha = 0.1, 1$ with different value of $H^2 = 0.5, 2, 16, 36, 49, 64$ agrees with the result of SSNM (sixth-order spline numerical method), see Figs. 10, 12, 3, and 4 of [29]. The numerical solution by BWSM and JWSM for different values of H^2 is given in Tables 1 and 2, respectively. The absolute residual errors and CPU time for different values of J are shown in Table 3.

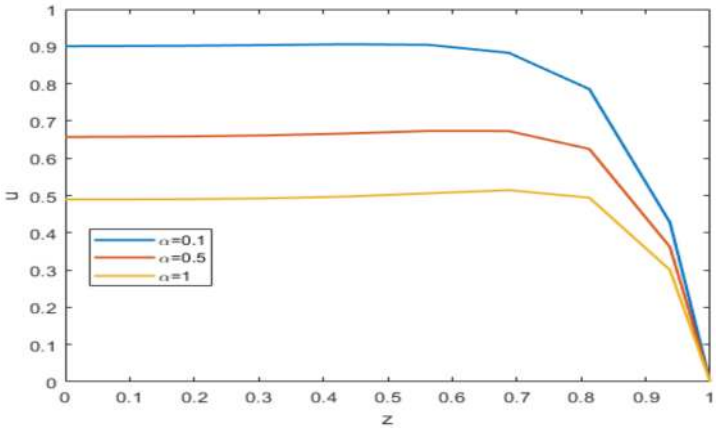

Figure 5 Graph of BWSM solution of EHD equation for $J = 3$, $M = 8$ and $k = 1$, $H^2 = 100$

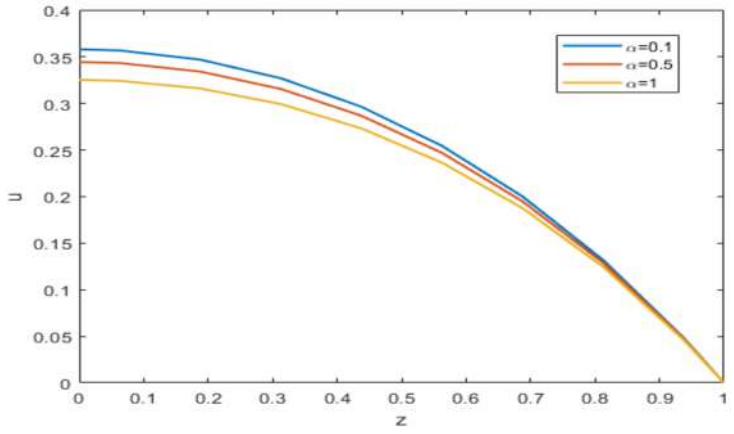

Figure 6 Graph of JWSM solution of EHD equation for $J = 3$, $M = 8$ and $k = 1$, $H^2 = 2$

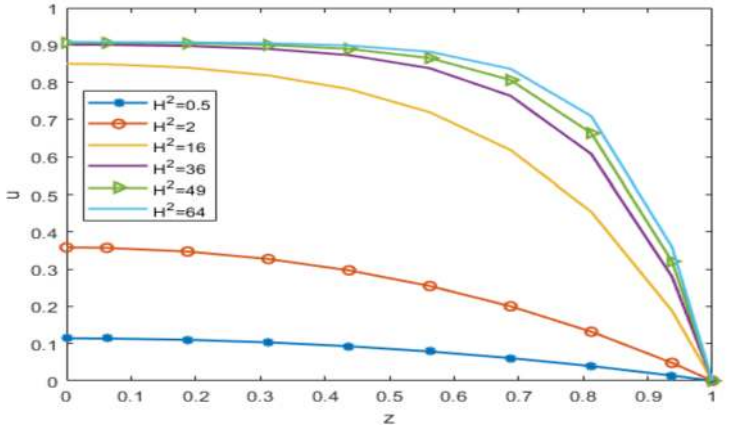

Figure 7 Graph of BWSM solution of EHD equation for $J = 3$, $M = 8$ and $k = 1$, $\alpha = 0.1$

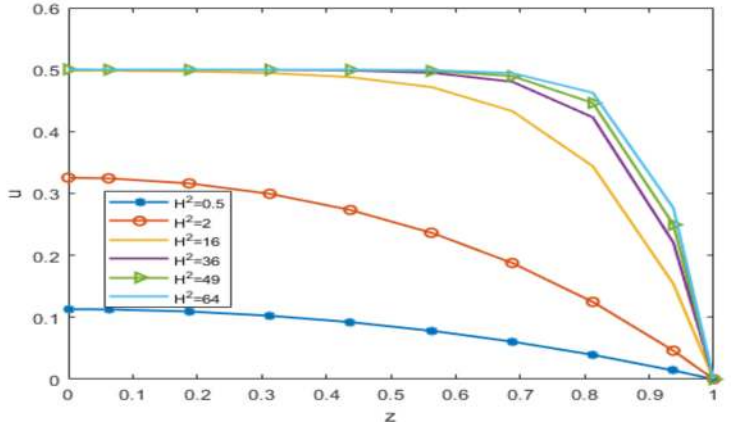

Figure 8 Graph of JWSM solution of EHD equation for $J = 3$, $M = 8$ and $k = 1$, $\alpha = 1$

Table 1 BWSM solution of EHM equation for $\alpha = 0.1$ with $J = 3$, $M = 8$, $k = 1$

z	$H^2 = 0.5$	$H^2 = 2$	$H^2 = 16$	$H^2 = 36$	$H^2 = 49$
0	0.1141	0.3583	0.8498	0.9010	0.9062
0.0625	0.1137	0.3571	0.8487	0.9006	0.9060
0.1875	0.1102	0.3472	0.8394	0.8976	0.9044
0.3125	0.1033	0.3272	0.8186	0.8898	0.9001
0.4375	0.0928	0.2966	0.7816	0.8730	0.8898
0.5625	0.0788	0.2546	0.7196	0.8377	0.8652
0.6875	0.0611	0.2002	0.6182	0.7636	0.8060
0.8125	0.0396	0.1320	0.4537	0.6075	0.6635
0.9375	0.0142	0.0483	0.1881	0.2795	0.3207
1	0	0	0	0	0

Table 2 JWSM solution of EHD equation for $\alpha = 1$ with $J = 3$, $M = 8$, $k = 1$

z	$H^2 = 0.5$	$H^2 = 2$	$H^2 = 16$	$H^2 = 36$	$H^2 = 49$
0	0.1132	0.3255	0.4984	0.5003	0.5004
0.0625	0.1128	0.3244	0.4982	0.5000	0.5000
0.1875	0.1094	0.3163	0.4973	0.4999	0.4999
0.3125	0.1025	0.2995	0.4946	0.4997	0.4999
0.4375	0.0922	0.2733	0.4879	0.4988	0.4996
0.5625	0.0783	0.2366	0.4718	0.4951	0.4980
0.6875	0.0607	0.1877	0.4331	0.4805	0.4896
0.8125	0.0394	0.1248	0.3440	0.4230	0.4463
0.9375	0.0141	0.0460	0.1540	0.2204	0.2495
1	0	0	0	0	0

Table 3 Maximum absolute residual errors of EHD equation for $\alpha = 1$ and $H^2 = 0.5$

J	JWSM	CPU time	BWSM	CPU time
3	5.5511e−15	0.38 seconds	4.2466e−14	0.9 seconds
4	5.1070e−15	0.49 seconds	9.9920e−16	2 seconds

6.2 Numerical treatment of nonlinear heat conduction model in the human head

Consider equation (1.4) along with boundary conditions (1.5) and $p(u) = e^{-u}$, $\gamma = 1$, $\nu = 1$, $\mu = 2$, and $u_k = 0$ and get the following Emden–Fowler type equation:

$$u''(z) + \frac{2}{z}u'(z) + e^{-u} = 0, \tag{6.1}$$

and the boundary conditions become

$$u'(0) = 0; \qquad u'(1) + 2u(1) = 0. \tag{6.2}$$

We used Bernoulli and Jacobi wavelets for solving this problem. The calculation has been done by taking $\kappa = -\frac{1}{4}$ and $\omega = -\frac{1}{3}$ in Jacobi wavelet. A comparison of our results with the results of Haar solution [35] and ADM [36] is given in Table 4. We show the absolute residual errors and CPU time for different J in Table 5. Figures 9 and 10 show the BWSM and JWSM solution at $J = 3$ for different values of γ, respectively.

6.3 Numerical treatment of spherical catalyst equation

Consider equation (1.6) with (1.7) by taking $\beta = 1$, $\rho = 1$. We have performed BWSM and JWSM ($\kappa = \frac{1}{5}, \omega = -\frac{1}{6}$) for the solution of (1.6). The influence of different values of

Table 4 Numerical solution of nonlinear heat conduction model in the human head for $\gamma = 1$ with $J = 3, M = 8, k = 1$

z	BWSM	JWSM	Haar [35]	ADM [36]
0	0.2700	0.2700	–	–
0.1	0.2688	0.2688	0.26866	0.26862
0.2	0.2649	0.2649	0.26484	0.26480
0.3	0.2585	0.2585	0.25845	0.25841
0.4	0.2495	0.2495	0.24945	0.24943
0.5	0.2379	0.2379	0.23782	0.23781
0.6	0.2236	0.2236	0.22349	0.22349
0.7	0.2065	0.2065	0.20640	0.20641
0.8	0.1866	0.1866	0.18646	0.18648
0.9	0.1637	0.1637	0.16356	0.16359

Table 5 Maximum absolute residual errors of nonlinear heat conduction model for $\gamma = 1$

J	JWSM	CPU time	BWSM	CPU time
3	1.6263e–12	0.4 seconds	2.1283e–13	1.4 seconds
4	8.7896e–13	0.5 seconds	8.6597e–15	2 seconds

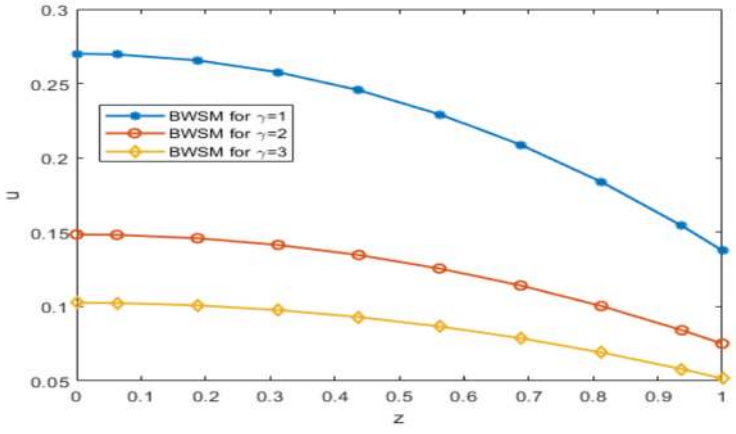

Figure 9 Graph of BWSM solution of nonlinear heat conduction model in human head equation for different γ with $J = 3, M = 8$, and $k = 1$

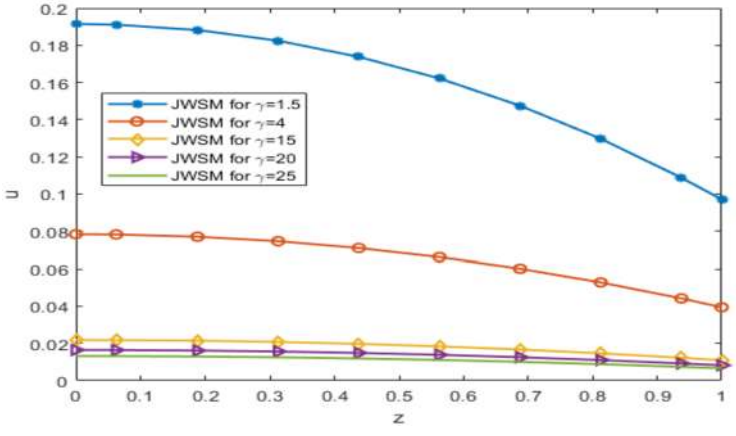

Figure 10 Graph of JWSM solution of nonlinear heat conduction model in human head equation for different γ with $J = 3, M = 8$, and $k = 1$

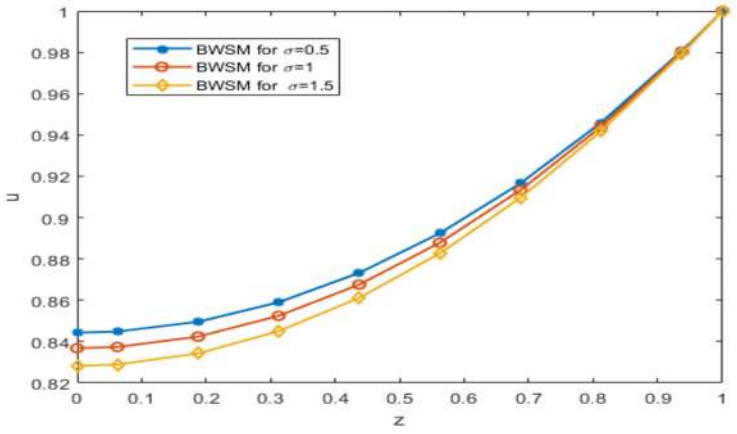

Figure 11 Graph of BWSM solution of spherical catalyst equation for $J = 3$, $M = 8$ and $k = 1$, $\sigma = 0.5, 1, 1.5$

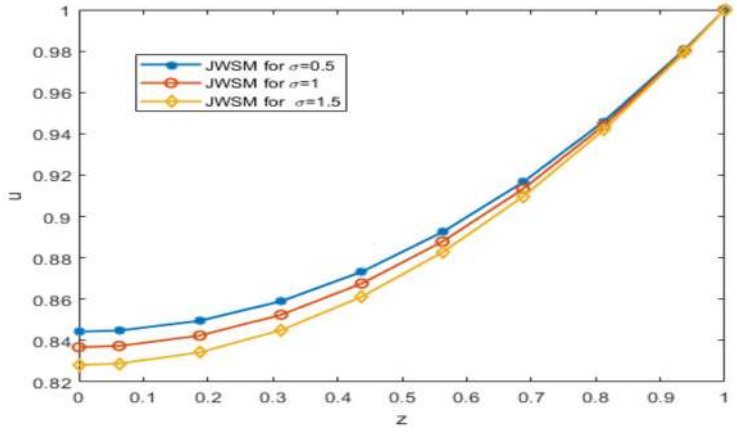

Figure 12 Graph of JWSM solution of spherical catalyst equation for $J = 3$, $M = 8$ and $k = 1$, $\sigma = 0.5, 1, 1.5$

Table 6 Numerical solution of spherical catalyst equation for $\beta = 1$, $\rho = 1$ with $J = 3$, $M = 8$, $k = 1$

z	BWSM ($\sigma = 0.5$)	BWSM ($\sigma = 1$)	JWSM ($\sigma = 1.5$)	OHAM [34] ($\sigma = 0.5$)	OHAM [34] ($\sigma = 1.5$)
0	0.8443	0.8368	0.8282	–	–
0.1	0.8458	0.8384	0.8299	0.8457	0.8299
0.2	0.8503	0.8432	0.8351	0.8502	0.8351
0.3	0.8579	0.8512	0.8437	0.8578	0.8437
0.4	0.8685	0.8625	0.8558	0.8684	0.8557
0.5	0.8822	0.8771	0.8713	0.8822	0.8712
0.6	0.8991	0.8950	0.8902	0.8991	0.8902
0.7	0.9193	0.9162	0.9126	0.9193	0.9126
0.8	0.9428	0.9407	0.9384	0.9427	0.9383
0.9	0.9696	0.9687	0.9675	0.9696	0.9675

activation energy is shown in Figs. 11 and 12. The numerical solution of (1.6) for $\sigma = 0.5, 1, 1.5$ is given in Table 6. We compare our results with the results of OHAM [29] in Table 7.

Table 7 Maximum absolute residual errors of spherical catalyst equation for $\beta = \rho = 1$ with $J = 2$

σ	OHAM [34]	JWSM	CPU time	BWSM	CPU time
0.5	5.66e–05	1.1768e–14	0.4 seconds	2.5158e–13	0.5 seconds
1	4.75e–05	1.0628e–12	0.5 seconds	2.9277e–12	0.5 seconds
1.5	4.28e–04	1.6083e–11	0.4 seconds	7.4860e–12	0.5 seconds

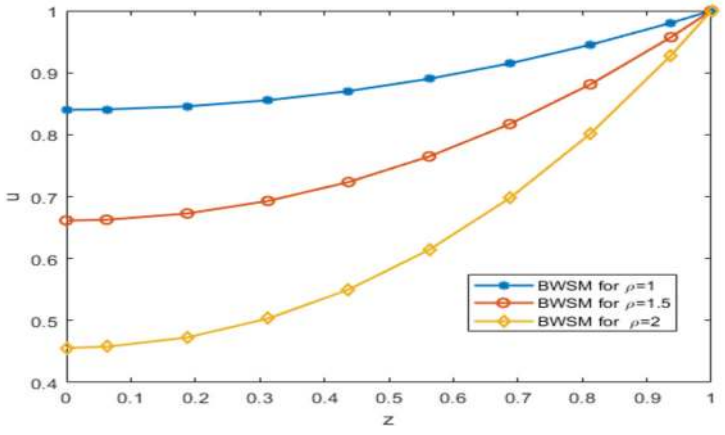

Figure 13 Graph of BWSM solution of spherical biocatalyst equation for $J = 3$, $M = 8$ and $k = 1$, $\beta = 2$

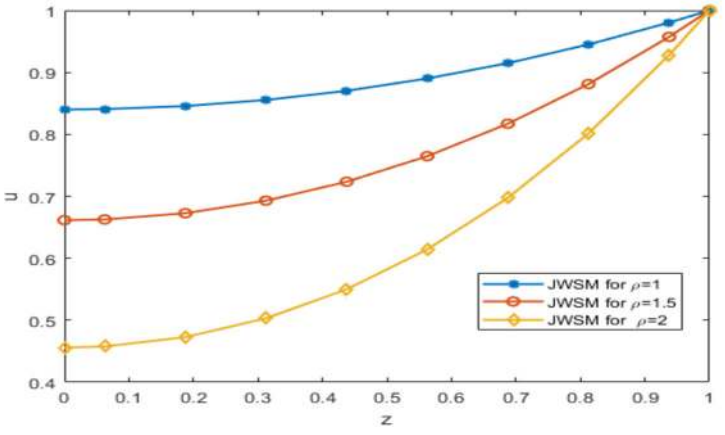

Figure 14 Graph of JWSM solution of spherical biocatalyst equation for $J = 3$, $M = 8$ and $k = 1$, $\beta = 2$

6.4 Numerical treatment of spherical biocatalyst equation

Consider equation (1.8) with (1.9) by fixing $\beta = 2$. We have performed BWSM and JWSM ($\kappa = \frac{-3}{5}, \omega = -\frac{1}{8}$) for the solution of (1.8). The influence of different values of Thiele modulus is shown in Figs. 13 and 14. The numerical solution of (1.6) for $\rho = 1, 1.5, 2$ is given in Table 8. We compare our results with the results of OHAM [34] in Table 9.

7 Conclusion

In this paper, we have studied EHD flow in a charged circular cylinder conduit, nonlinear heat conduction model in the human head, non-isothermal reaction–diffusion model equations in a spherical catalyst, and non-isothermal reaction–diffusion model equations

Table 8 Numerical solution of spherical biocatalyst equation for $\beta = 2$ with $J = 3$, $M = 8$, $k = 1$

z	BWSM ($\rho = 1$)	BWSM ($\rho = 1.5$)	JWSM ($\rho = 2$)	OHAM [34] ($\rho = 1$)	OHAM [34] ($\rho = 1.5$)
0	0.8401	0.6615	0.4559	–	–
0.1	0.8417	0.6647	0.4607	0.8417	0.6646
0.2	0.8464	0.6743	0.4751	0.8464	0.6743
0.3	0.8543	0.6905	0.4994	0.8542	0.6904
0.4	0.8653	0.7132	0.5342	0.8653	0.7132
0.5	0.8795	0.7428	0.5798	0.8795	0.7427
0.6	0.8970	0.7793	0.6372	0.8969	0.7793
0.7	0.9177	0.8230	0.7070	0.9177	0.8230
0.8	0.9418	0.8742	0.7902	0.9417	0.8741
0.9	0.9692	0.9331	0.8875	0.9691	0.9330

Table 9 Maximum absolute residual errors of spherical biocatalyst equation for $\beta = 2$ with $J = 2$

ρ	OHAM [34]	JWSM	CPU time	BWSM	CPU time
1	1.21e–06	8.8425e–08	0.4 seconds	5.6621e–15	0.5 seconds
2	1.98e–06	7.8504e–08	0.6 seconds	6.2004e–10	0.6 seconds
3	6.02e–04	2.2560e–13	0.5 seconds	1.9376e–12	0.5 seconds

in a spherical biocatalyst which are modeled by Lane–Emden type equations having strong nonlinearity. We have solved these models by two numerical methods based on Jacobi and Bernoulli wavelets. These wavelet methods solved Lane–Emden type equations by converting them into a system of nonlinear equations. In the study of EHD flow, we observed that the effects of Hartmann number and nonlinearity have an important impact. Further we also compare our results with the results of SSNM [29], Haar [35], ADM [36], and OHAM [34]. The graphs show the efficiency of our methods. Moreover, the present semi-analytical numerical methods have lower computational cost than ADM, Haar, and OHAM, since in our methods there is no need for symbolic successive integration which is computationally higher than numerical methods.

Acknowledgements
The authors are indebted to the anonymous reviewer for his helpful, valuable comments and suggestions in the improvement of the manuscript. First author is thankful to Council of Scientific and Industrial Research (CSIR), Govt. of India, for providing Junior Research Fellowship.

Funding
Not applicable.

Availability of data and materials
Not applicable.

Competing interests
The authors declare that they have no competing interests.

Authors' contributions
All authors drafted the manuscript, and they read and approved the final version.

Author details
[1]Department of Mathematics, Jamia Millia Islamia, New Delhi, 110025, India. [2]Department of Mathematics, College of Sciences and Humanities in Al-Kharj, Prince Sattam bin Abdulaziz University, Alkharj 11942, Saudi Arabia. [3]Department of Basic Engineering Science, Faculty of Engineering, Menoufia University, Shebin El-Kom 32511, Egypt.

Received: 9 June 2020 Accepted: 10 September 2020 Published online: 25 September 2020

References

1. Azodi, H.D.: Numerical solution of fractional-order sir epidemic model via Jacobi wavelets. J. Int. Math. Virtual Inst. **10**(1), 183–197 (2020)
2. Duggan, R.C., Goodman, A.M.: Pointwise bounds for a nonlinear heat conduction model of the human head. Bull. Math. Biol. **48**(2), 229–236 (1986)
3. El-Kabeir, S.M.M., El-Zahar, E.R., Modather, M., Gorla, R.S.R., Rashad, A.M.: Unsteady MHD slip flow of a ferrofluid over an impulsively stretched vertical surface. AIP Adv. **9**(4), 045112 (2019)
4. El-Zahar, E.R., Rashad, A.M., Saad, W., Seddek, L.F.: Magneto-hybrid nanofluids flow via mixed convection past a radiative circular cylinder. Sci. Rep. **10**(1), 1–13 (2020)
5. Fylladitakis, E.D., Theodoridis, M.P., Moronis, A.X.: Review on the history, research and application of electrohydrodynamics. IEEE Trans. Plasma Sci. **42**(2), 358–375 (2014)
6. Ghasemi, S.E., Hatami, M., Ahangar, G.R.M., Ganji, D.D.: Electrohydrodynamic flow analysis in a circular cylindrical conduit using least square method. J. Electrost. **72**, 47–52 (2014)
7. Hossmann, K.-A., Hermann, D.M.: Effects of electromagnetic radiation of mobile phones on the central nervous system. Bioelectromagnetics **24**(1), 49–62 (2003)
8. Jamal, B., Khuri, S.A.: Non-isothermal reaction–diffusion model equations in a spherical biocatalyst:Green's function and fixed point iteration approach. Int. J. Appl. Comput. Math. **5**(4), 120 (2019). https://doi.org/10.1007/s40819-019-0704-1
9. Keangin, P., Rattanadecho, P., Wessapan, T.: An analysis of heat transfer in liver tissue during microwave ablation using single and 2 double slot antenna. Int. Commun. Heat Mass Transf. **38**, 757–766 (2011)
10. Keshavarz, E., Ordokhani, Y., Razzaghi, M.: Numerical solution of nonlinear mixed Fredholm–Volterra integro-differential equations of fractional order by Bernoulli wavelets. Comput. Methods Differ. Equ. **7**(2), 163–176 (2019)
11. Ketley, V., Wood, A.W., Spoung, J., Stough, C.: Neuropsychological sequelae of digital mobile phone exposure in humans. Neuropsychologia **44**(10), 1843–1848 (2006)
12. Lin, L.: Cataracts and personal communication radiation. IEEE Microw. Mag. **4**, 26–32 (2003)
13. Lindholm, H., Alanko, T., Rintamäki, H.: Thermal effects of mobile phone RF fields on children: a provacation study. Prog. Biophys. Mol. Biol. **107**(3), 399–403 (2011)
14. Madduri, H., Roul, P.: A fast-converging iterative scheme for solving a system of Lane–Emden equations arising in catalytic diffusion reactions. J. Math. Chem. **57**(2), 570–582 (2019)
15. Mastroberardino, A.: Homotopy analysis method applied to electrohydrodynamic flow. Commun. Nonlinear Sci. Numer. Simul. **16**, 2730–2736 (2011)
16. Mckee, S., Watson, R., Cuminato, J.A., Caldwell, J., Chen, M.S.: Calculation of electro-hydrodynamic flow in a circular cylindrical conduit. Z. Angew. Math. Mech. **77**, 457–465 (1997)
17. Mosayebidorcheh, S.: Taylor series solution of the electrohydrodynamic flow equation. J. Mech. Eng. Technol. **1**(2), 40–45 (2013)
18. Rach, R., Duan, J.S., Wazwaz, A.M.: Solving coupled Lane–Emden boundary value problems in catalytic diffusion reactions by the Adomian decomposition method. J. Math. Chem. **52**(1), 255–267 (2014)
19. Rach, R., Duan, J.S., Wazwaz, A.M.: On the solution of non-isothermal reaction–diffusion model equations in a spherical catalyst by the modified Adomian method. Chem. Eng. Commun. **202**(8), 1081–1088 (2015)
20. Rong, L.J., Phang, C.: Jacobi wavelet operational matrix of fractional integration for solving fractional integro-differential equation. J. Phys. Conf. Ser. **693**, 012002 (2016)
21. Roul, P.: An improved iterative technique for solving nonlinear doubly singular two-point boundary value problems. Eur. Phys. J. Plus **131**(6), 1–15 (2016)
22. Roul, P.: Doubly singular boundary value problems with derivative dependent source function: a fast-converging iterative approach. Math. Methods Appl. Sci. **42**(1), 354–374 (2019)
23. Roul, P.: A new mixed MADM-collocation approach for solving a class of Lane–Emden singular boundary value problems. J. Math. Chem. **57**(3), 945–969 (2019)
24. Roul, P.: A fourth-order non-uniform mesh optimal B-spline collocation method for solving a strongly nonlinear singular boundary value problem describing electrohydrodynamic flow of a fluid. Appl. Numer. Math. (2020). https://doi.org/10.1016/j.apnum.2020.03.018
25. Roul, P., Goura, V.P., Agarwal, R.: A compact finite difference method for a general class of nonlinear singular boundary value problems with Neumann and Robin boundary conditions. Appl. Math. Comput. **350**, 283–304 (2019)
26. Roul, P., Madduri, H.: A new highly accurate domain decomposition optimal homotopy analysis method and its convergence for singular boundary value problems. Math. Methods Appl. Sci. **41**(16), 6625–6644 (2018)
27. Roul, P., Madduri, H., Agarwal, R.: A fast-converging recursive approach for Lane–Emden type initial value problems arising in astrophysics. J. Comput. Appl. Math. **359**, 182–195 (2019)
28. Roul, P., Madduri, H., Kassner, K.: A new iterative algorithm for a strongly nonlinear singular boundary value problem. J. Comput. Appl. Math. **351**, 167–178 (2019)
29. Roul, P., Madduri, H., Kassner, K.: A sixth-order numerical method for a strongly nonlinear singular boundary value problem governing electrohydrodynamic flow in a circular cylindrical conduit. Appl. Math. Comput. **350**, 416–433 (2019)
30. Roul, P., Thula, K.: A fourth-order B-spline collocation method and its error analysis for Bratu-type and Lane–Emden problems. Int. J. Comput. Math. **96**(1), 85–104 (2019)
31. Roul, P., Thula, K., Agarwal, R.: Non-optimal fourth-order and optimal sixth-order B-spline collocation methods for Lane–Emden boundary value problems. Appl. Numer. Math. **145**, 342–360 (2019)
32. Roul, P., Thula, K., Goura, V.P.: An optimal sixth-order quartic B-spline collocation method for solving Bratu-type and Lane–Emden-type problems. Math. Methods Appl. Sci. **42**(8), 2613–2630 (2019)
33. Roul, P., Warbhe, U.: A new homotopy perturbation scheme for solving singular boundary value problems arising in various physical models. Z. Naturforsch. A **72**(8), 733–743 (2017)
34. Singh, R.: Optimal homotopy analysis method for the non-isothermal reaction–diffusion model equations in a spherical catalyst. J. Math. Chem. **56**(9), 2579–2590 (2018)

35. Singh, R., Guleria, V., Singh, M.: Haar wavelet quasilinearization method for numerical solution of Emden–Fowler type equations. Math. Comput. Simul. **174**, 123–133 (2020)
36. Singh, R., Kumar, J.: An efficient numerical technique for the solution of nonlinear singular boundary value problems. Comput. Phys. Commun. **185**(4), 1282–1289 (2014)
37. Tullis, T.K., Bayazitoglu, Y.: Analysis of relaxation times on the human head using the thermal wave model. Int. J. Heat Mass Transf. **67**, 1007–1013 (2013)
38. Van Gorder, R.A.: Exact first integrals for a Lane–Emden equation of the second kind modeling a thermal explosion in a rectangular slab. New Astron. **16**(8), 492–497 (2011)
39. Wainwright, P.: Thermal effects of radiation from cellular telephones. Phys. Med. Biol. **45**(8), 2363–2372 (2000)
40. Wazwaz, A.M.: The variational iteration method for solving new fourth-order Emden–Fowler type equations. Chem. Eng. Commun. **202**(11), 1425–1437 (2015)
41. Wazwaz, A.M.: Solving the non-isothermal reaction–diffusion model equations in a spherical catalyst by the variational iteration method. Chem. Phys. Lett. **679**, 132–136 (2017)
42. Wessapan, T., Rattanadecho, P.: Numerical analysis of specific absorption rate and heat transfer in human head subjected to mobile phone radiation: effects of user age and radiated power. J. Heat Transf. **134**, 121101 (2012)
43. Wessapan, T., Srisawatdhisukul, S., Rattanadecho, P.: Numerical analysis of specific absorption rate and heat transfer in the human body exposed to leakage electromagnetic field at 915 MHz and 2450 MHz. ASME J. Heat Transfer. **133**, 051101 (2011)
44. Wessapan, T., Srisawatdhisukul, S., Rattanadecho, P.: Specific absorption rate and temperature distributions in human head subjected to mobile phone radiation at different frequencies. Int. J. Heat Mass Transf. **55**(1–3), 347–359 (2012)
45. Xiaopeng, C., Jiusheng, C., Xiezhen, Y.: Advances and applications of electrohydrodynamics. Chin. Sci. Bull. **48**, 1055–1063 (2003)
46. Zogheib, B., Tohidi, E., Shateyi, S.: Bernoulli collocation method for solving linear multidimensional diffusion and wave equations with Dirichlet boundary conditions. Adv. Math. Phys. **2017**, Article ID 5691452 (2017). https://doi.org/10.1155/2017/5691452